Eur. J. Biochem. *151*, 153–165 (1985)

The structure of the double-stranded RNA pentamer 5′(CACAG) · 5′(CUGUG) determined by nuclear Overhauser enhancement measurements: Interproton distance determination and structure refinement on the basis of X-ray coordinates

G. Marius CLORE[1], Angela M. GRONENBORN[1] and Larry W. McLAUGHLIN[2]

[1] Max-Planck-Institut für Biochemie, Martinsried bei München
[2] Max-Planck-Institut für Experimentelle Medizin, Abteilung Chemie, Göttingen

(Received January 21/April 24, 1985) – EJB 85 0042

The structure in solution of the duplex RNA pentamer 5′(CACAG) · 5′(CUGUG), comprising the stem of the TΨC loop of yeast $tRNA^{Phe}$, has been investigated by means of one- and two-dimensional nuclear Overhauser enhancement measurements. All non-exchangeable base and sugar proton resonances with the exception of the H5′/H5″ sugar resonances are assigned in a sequential manner. From the relative intensities of the cross-peaks obtained in the pure-phase absorption two-dimensional nuclear Overhauser enhancement spectra at several mixing times, it is deduced that the RNA pentamer adopts an A-type conformation in solution. Cross-relaxation rates and interproton distances are determined from the time dependence of the nuclear Overhauser effects, principally by one-dimensional measurements. The structure of the RNA pentamer is then refined by restrained least-squares minimization on the basis of both distance and planarity restraints using fibre diffraction data as an initial model. The refined structure of the RNA pentamer is of the A type but exhibits local structural variations in glycosidic bond and backbone torsion angles as well as in propellor twist, base roll and base tilt angles.

Over the last few years numerous NMR studies have appeared on the structure of small DNA oligonucleotides in solution (see [1–4] for reviews). In contrast, relatively few studies have appeared on RNA duplexes [5–9]. This is probably due to two factors, both of which arise from the presence of the 2′-hydroxyl group in RNA. First, RNA is intrinsically more difficult to synthesize than DNA as an additional reactive group has to be protected during the course of the synthesis [10, 11]. Second, all the sugar resonances, with the exception of the H1′ resonances, are superimposed in a very narrow region of the ^{1}H-NMR spectrum only 1 ppm in width, thereby considerably complicating the task of resonance assignment. As part of our continuing studies on the structure and dynamics of oligonucleotides in solutions (see for examples [4, 8, 12–16]), we present a 500-MHz NMR study on the double-stranded RNA pentamer

$$\begin{array}{llllllll} 5' & C_1 & -A_2 & -C_3 & -A_4 & -G_5 & 3' \\ & \cdot & \cdot & \cdot & \cdot & \cdot & \\ 3' & G_{10} & -U_9 & -G_8 & -U_7 & -C_6 & 5' \end{array}$$

comprising the stem of the TΨC loop of yeast $tRNA^{Phe}$. The non-exchangeable proton resonances are assigned in a sequential manner by means of two-dimensional pure-phase absorption nuclear Overhauser enhancement spectroscopy (NOESY). Cross-relaxation rates and interproton distances are then determined from the time dependence of the nuclear Overhauser effects (NOE), principally using one-dimensional measurements. Finally the structure of the RNA is refined by restrained least-squares minimization on the basis of distance and planarity restraints. The refined structure of the RNA pentamer is that of A-RNA but exhibits local structural variations in glycosidic bond and backbone torsion angles as well as in propellor twist, base roll and base tilt angles.

Correspondence to G. M. Clore, Max-Planck-Institut für Biochemie, D-8033 Martinsried bei München, Federal Republic of Germany

Abbreviations. NOE, nuclear Overhauser enhancement; NOESY, two-dimensional nuclear Overhauser enhancement spectroscopy; CD, circular dichroism; RMS, root-mean-square.

EXPERIMENTAL PROCEDURE

The two RNA pentamers (5′)CpApCpApG and (5′)-CpUpGpUpG were synthesized using the bifunctional phosphorylating agent *o*-chlorophenyl-*O*,*O*-bis(1-benzotriazolyl) phosphate [17]. The exocyclic amine groups of guanosine, adenosine and cytidine were protected as benzoyl, benzoyl and anisoyl amides respectively. The 2′-hydroxyl functions were protected as the tetrahydropyranyl ethers except for the 3′-terminal residues which contained 2′,3′-dibenzoyl-protected ribose moieties. The 5′-terminal hydroxyl was in each case protected as the 4,4′-dimethoxytrityl derivative. The fully protected products were deprotected in three consecutive steps essentially as described elsewhere [18] but without intermediate purification. The fully deprotected products were purified by high-pressure liquid chromatography as described by McLaughlin and Piel [19]. The products were analysed as described previously [20].

The samples for ^{1}H-NMR spectroscopy were freeze-dried extensively from 99.6% D_2O and finally dissolved in 99.96% D_2O buffer containing 500 mM KCl, 50 mM potassium phosphate pH* 6.5 (meter reading uncorrected for the isotope effect on the glass electrode) and 0.1 mM EDTA. The concentration of duplex pentamer used was 8 mM. All glassware was heated to 200 °C for 4 h before use to inactive possible traces of ribonuclease.

^{1}H-NMR spectra were recorded at 500 MHz on a Bruker AM 500 spectrometer equipped with an ASPECT 3000 computer. Chemical shifts are expressed relative to 4,4-dimethylsilapentane-1-sulphonate. All measurements were carried out at 21 °C.

NOESY spectra [21] were recorded in pure-phase absorption mode using the method of Marion and Wüthrich [22]. Appropriate phase cycling was used for the suppression of axial peaks and of cross-peaks due to coherence transfer via multiple quantum coherence; in addition a 15% random variation in the mixing time τ_m was used to eliminate zero-quantum coherence transfer [23]. The spectral width in the F1 and F2 dimensions was 5000 Hz with the carrier placed in the middle of the spectrum, and 128 transients were collected for each of 600 increments with a relaxation delay of 1 s between successive transients. A square $1K \times 1K$ frequency domain matrix was obtained by zero-filling in t_1 to give a digital resolution of 4.88 Hz per point in each domain. An initial phase correction was carried out during transformation with a final adjustment after completion of the two-dimensional transformation. These manipulations were followed by symmetrization.

One-dimensional NOE spectra were recorded with a 90° observation pulse, an acquisition time of 0.5 s (8 K data points and an 8.2-kHz spectral width) and a relaxation delay of 2 s. The NOEs were observed by directly collecting the difference free induction decay by interleaving eight transients after saturation for a set time of a given resonance with eight transients of off-resonance irradiation (applied for the same length of time), negating the memory between eight transient cycles. The irradiation power used was sufficient to be in the high power limit so that saturation was effectively instantaneous whilst selectivity was preserved so that only a single resonance at a time was saturated [24]. 800 transients were recorded for each difference spectrum and prior to Fourier transformation the difference free induction decays were multiplied by an exponential equivalent to a line broadening of 2 Hz.

Restrained least-squares refinement was carried out using the crystallographic refinement program RESTRAIN [25–27] which makes use of the Gauss-Seidel iterative method to solve the least-squares normal equations in cartesian coordinate space.

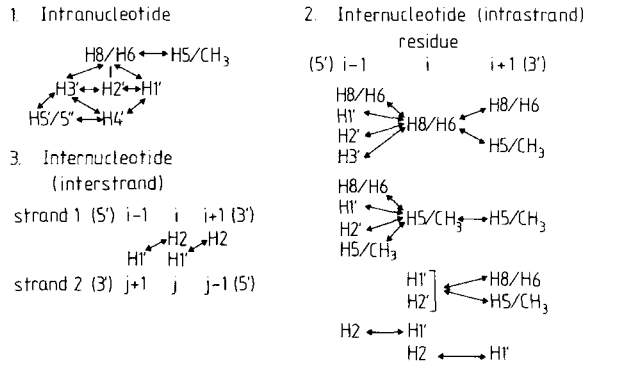

Fig. 1. *Scheme used for the sequential assignment of non-exchangeable proton resonances in right-handed RNA oligonucleotides*

RESULTS AND DISCUSSION

Sequential resonance assignment

All experiments were carried out at 21 °C in a D_2O buffer containing 500 mM KCl and 50 mM potassium phosphate pH* 6.5. Under these conditions of temperature and ionic strength the RNA pentamer is entirely double stranded as judged by the presence of all five exchangeable imino proton resonances in the spectrum in H_2O (not shown) and by the temperature dependence of the chemical shifts (melting temperature ≈ 40 °C).

The assignment of the non-exchangeable proton resonances was accomplished by means of NOE measurements on a sequential basis using the scheme outlined in Fig. 1. This is based on the known structures of right-handed nucleic acids [28] and makes no assumption of A or B type geometry [4, 12, 16, 29–36]. A series of contour plots illustrating various regions of the pure phase absorption NOESY spectra are shown in Figs 2–4. The H8/H6 base protons and H1′ sugar protons are assigned via the H1′(*i*-1) ↔ H8/H6(*i*) ↔ H1′(*i*) NOE pathway (Fig. 2). The H5 resonances of the C and U residues are then easily assigned through the intranucleotide H5 ↔ H6 NOEs (Fig. 2). The A(H2) resonances are assigned by both intra- and interstrand NOEs involving the H1′ sugar resonances: each H2 proton gives an NOE to the H1′ proton of the residue of the same strand on its 3′ side and to the H1′ proton of the residue of the opposite strand on its 5′ side (Fig. 2). The H2′ and H4′ resonances can then be assigned through the intranucleotide H1′-H2′ and H1′-H4′ NOEs, as for all sugar pucker conformations the closest sugar proton to the H1′ proton is the H2′ proton of the same residue followed by the H4′ proton of the same residue (Fig. 3). The assignments of the H2′ resonances can then be confirmed through the sequential H2′(*i*-1) ↔ H8/H6(*i*) ↔ H2′(*i*) NOE pathway (Fig. 4). Finally, the H3′ resonances can be assigned through intranucleotide H2′-H3′ and H8/H6-H3′ NOEs, as well as some internucleotide H3′(*i*-1)-H8/H6(*i*) NOEs (Fig. 4). Unfortunately, the assignment of the H5′ and H5″ resonances, with the exception of those arising from the residues at the 5′ terminus (*viz.* C_1 and C_6), presents an intractable problem as there are no connectivities involving well resolved resonances. The H5′/H5″ resonances of the residues of the 5′ terminus always lie upfield of the main bulk of the H2′/H3′/H4′/H5′/H5″ resonances, the H5′ and H5″ resonances of residues C_1 and C_6 being superimposed at 3.75 ppm. The assignment of the base and sugar resonances are given in Table 1 and the observed internucleotide NOEs are summarized in Fig. 5.

Low-resolution solution structure

Because of the r^{-6} dependence of the NOE at short mixing times [24, 33–35] the relative cross-peak intensities provide a sensitive probe of conformation as monitored by short range (< 0.5 nm) interproton distances, and enable one to deduce a low resolution structure on the basis of a qualitative interpretation alone. Inspection of the relative intensities of the cross-peaks in the pure phase absorption NOESY spectra at 75 ms, 150 ms and 300 ms reveals the following general pattern of sugar-base NOEs: H8/H6(*i*)-H2′(*i*-1) > H8/H6(*i*)-H3′(*i*) > H8/H6(*i*)-H1′(*i*) ≈ H8/H6(*i*)-H1′(*i*-1) ≈ H2(*i*)-H1′(*i*+1) > H8/H6(*i*)-H2′(*i*). This pattern of NOEs is characteristic of a 3′-*endo* sugar pucker with a C4′-C3′ bond torsion angle δ in the range 80–90° and a low *anti* glycosidic bond torsion angle χ in the range −150° to −170°. These findings are characteristic of an A-type conformation in agreement with the A-type CD spectrum (data not shown). Also characteristic of this conformation are the interstranded NOEs between the H2 protons of residues A_2 and A_4 and the H1′ protons of

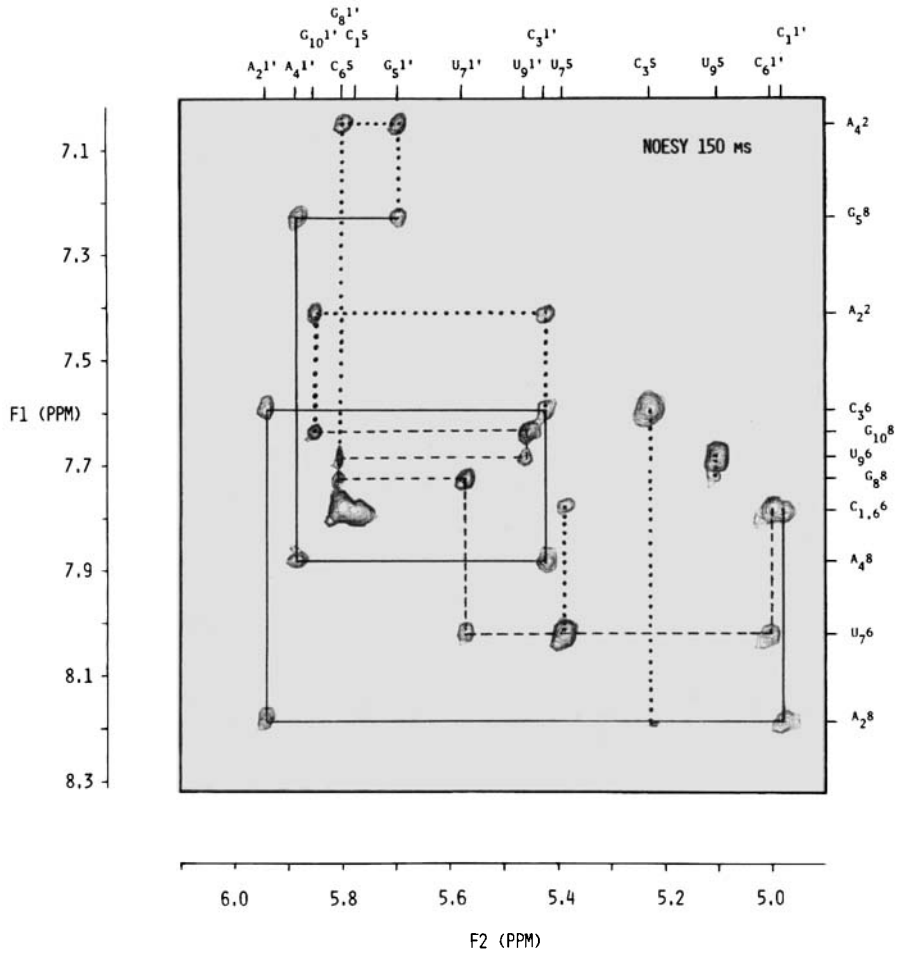

Fig. 2. *H8/H6 (F1 axis)-H1′/H5 (F2 axis) region of the pure-phase absorption NOESY spectrum at a mixing time of 150 ms.* The H1′(*i*-1)-H8/H6(*i*)-H1′(*i*) NOE connectivities are represented by continuous (———) and interrupted (– – – –) lines for strands 1 and 2 of the pentamer respectively. H8/H6(*i*-1)-H5(*i*), H2(*i*)-H1′(*i*+1) and the interstrand H2-H1′ connectivities are indicated by dotted lines (· · · · ·). Apodization and mild resolution enhancement were applied by multiplying the time-domain data with a sine-squared bell shifted by $\pi/6$ in both t_1 and t_2 dimensions

residues G_{10} and G_8 respectively, whose intensities are approximately the same as those of the intrastrand H2(*i*)-H1′(*i*+1) NOEs.

Interproton distances

In order to determine interproton distances, cross-relaxation rates were measured from the time dependence of the NOEs. We principally made use of one-dimensional NOE measurement as we found quantification more reliable and easier from one-dimensional than two-dimensional spectra. In those cases where two-dimensional integration of cross-peaks in the pure phase-absorption NOESY spectra was carried out, we found that the ratios of the initial slopes of the time courses of the cross-peak intensities were the same within experimental error as those for the corresponding NOEs obtained from the one-dimensional measurements. Some examples of NOE time courses are shown in Fig. 6. $(\langle r^{-6}\rangle)^{-1/6}$ mean interproton distances were then determined using the distance $r_{\text{H5-H6}}$ (0.246 nm) and mean cross-relaxation rate $\sigma_{\text{H5-H6}}$ between the H5 and H6 protons of the C and U residues as an internal reference from the equation [24, 37–39]:

$$(\langle r_{ij}^{-6}\rangle)^{-1/6} = (\sigma_{\text{H5-H6}}/\sigma_{ij})^{-1/6} \cdot r_{\text{H5-H6}} \qquad (1)$$

(where r_{ij} and σ_{ij} are the distance and cross-relaxation rate respectively between protons *i* and *j*) on the assumption that the effective correlation times of the *i*-*j* and intranucleotide H5-H6 interproton vectors are the same. The application of this equation has also been extensively used in other systems including proteins [40, 41], oligonucleotides [16, 42, 43], ligand-protein [44–46] and nucleic-acid – nucleic-acid [14, 15] interactions.

In using Eqn (1) several words of caution should be noted. First, if proton *i* is not only close to proton *j* but to other protons as well, such as say proton *k*, σ_{ij} can only be accurately determined from the initial slope of the time dependence of the NOE if either $\sigma_{ij} \gtrsim \sigma_{ik}$ or $\sigma_{ij} \gtrsim \sigma_{jk}$ [39]. Considerations of stereochemistry indicate that this condition is satisfied for all distances $\lesssim 0.3$ nm. Where this condition is not satisfied, a systematic error in the measured value of σ_{ij} and hence the calculated value of r_{ij} is incurred. In particular, the value of σ_{ij} will be overestimated. If the reference distance and cross-relaxation rate σ_{ref} are not part of the cross-relaxation network associated with σ_{ij}, then the value of r_{ij} will always be underestimated. If on the other hand the reference distance and cross-relaxation rate σ_{ref} are part of the cross-relaxation network associated with σ_{ij}, the sign of the systematic error in the estimation of r_{ij} depends on the relationship between σ_{ij} and σ_{ref}. Namely, r_{ij} will be overestimated if $\sigma_{ij} > \sigma_{\text{ref}}$ but

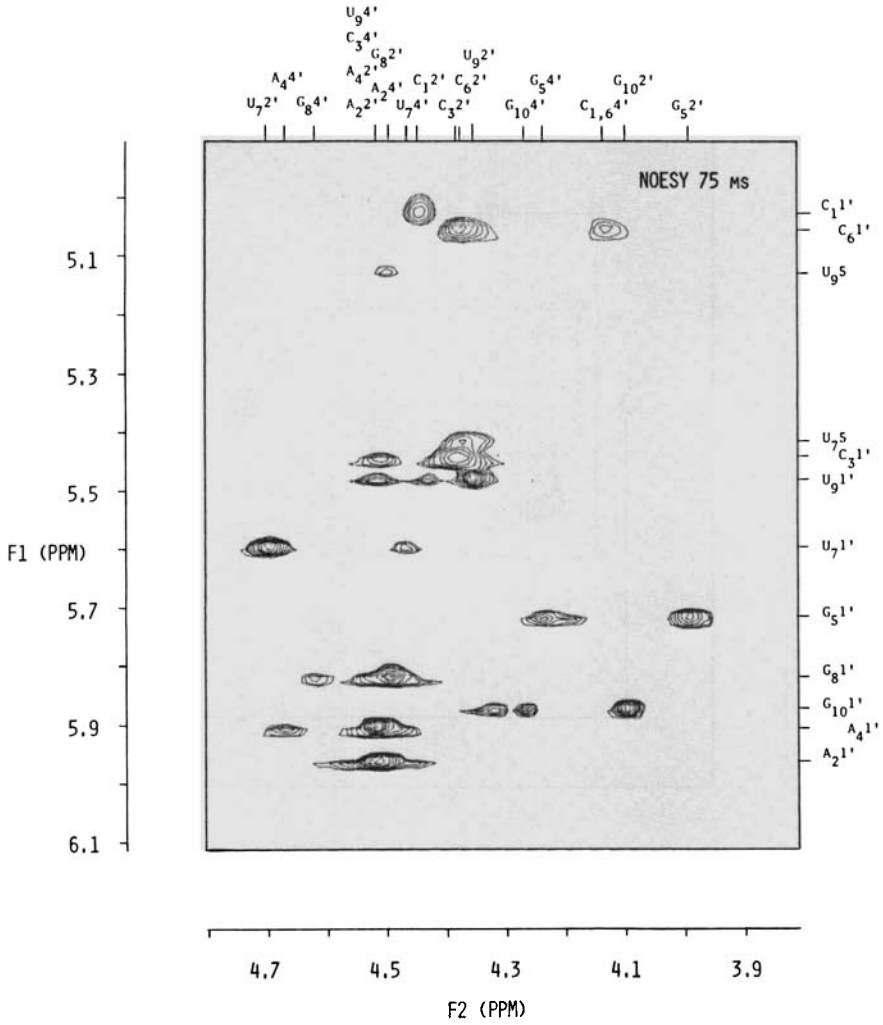

Fig. 3. *H1′/H5 (F1 axis)-H2′/H3′/H4′/H5′/H5″ (F2 axis) region of the pure-phase absorption NOESY spectrum at a mixing time of 75 ms.* Apodization was carried out by multiplying the time-domain data with a sine-squared bell shifted by $\pi/4$ in both t_1 and t_2 dimensions

underestimated if $\sigma_{ij} < \sigma_{ref}$. In general, however, these effects will be small. From the calculations of Clore and Gronenborn [39], it can be estimated that in the worst case for the present system involving the H1′(*i*-1)-H8/H6(*i*), H2′(*i*-1)-H8/H6(*i*) and H1′(*i*-1)-H2′(*i*-1) NOEs where $r_{H1'(i)\text{-}H2'(i)} \approx 0.25-0.27$ nm, $r_{H2'(i\text{-}1)\text{-}H8/H6(i)} \approx 0.21-0.25$ nm and $r_{H1'(i\text{-}1)\text{-}H8/H6(i)} \approx 0.33-0.35$ nm, the value of $r_{H1'(i\text{-}1)\text{-}H8/H6(i)}$ will at most suffer an underestimation of 0.01 nm when the initial slope of the NOEs are measured. The second cautionary note concerns potential variations in the effective correlation times τ_{eff} for different interproton vectors which may also lead to errors in the estimation of r_{ij}. When $\omega\tau_{eff} \gg 1$ (where ω is the spectrometer frequency) as in this case, the cross-relaxation rate σ_{ij} is not only proportional to $\langle r_{ij}^{-6} \rangle$ but also to the effective correlation time $\tau_{eff}(ij)$ of the *i*-*j* interproton vector. However, because of the $\langle r_{ij}^{-6} \rangle$ dependence of σ_{ij}, quite substantial variations in $\tau_{eff}(ij)$ relative to the effective correlation time τ_{eff}(ref) for the reference interproton vector only lead to relatively small errors in the estimation of r_{ij} using Eqn (1). Consider, for example, the case where σ_{ij} has a value of 0.5 s^{-1}, σ_{kl} a value of 1 s^{-1} and r_{kl} a value of 0.25 nm. Then for the three cases $\tau_{eff}(ij) = \tau_{eff}(kl)$, $\tau_{eff}(ij) = \tau_{eff}(kl)/2$ and $\tau_{eff}(ij) = 2\tau_{eff}(kl)$, r_{ij} is calculated to be 0.28 nm, 0.25 nm and 0.31 nm respectively. These three cases of course represent extreme variations in τ_{eff}. In the present case certain internal checks can be used to ascertain possible variations in effective correlation times. Thus, for example, within experimental error the intranucleotide H5-H6 base vector exhibits no residue-to-residue variation in cross-relaxation rate and hence effective correlation time (see Table 2). Of course, there may still be differences in internal mobility and effective correlation times between different components of each residue, *viz.* between the base and sugar moieties. Indeed, in the case of DNA oligonucleotides, it has been found that the effective correlation time for the intranucleotide H2′-H2″ sugar vector is a factor of approximately 3 times shorter than that of the intranucleotide H5-H6 base vector [47] and that this could lead to errors up to 0.05 nm if the inappropriate reference distance and cross-relaxation rate is used to calculate a particular unknown distance [16]. In the case of RNA there are no readily available fixed distance interproton vectors in the sugar ring to be able to check this in the same manner (note the cross-relaxation rate of the H5′-H5″ sugar vector cannot be measured due to spectral overcrowding). Nevertheless, there still exists a reliable handle with which to probe the mobility of the sugar ring relative to that of the base, namely the intranucleotide H1′-H2′ sugar vector which has a minimum value of about 0.25 nm when the sugar pucker is in

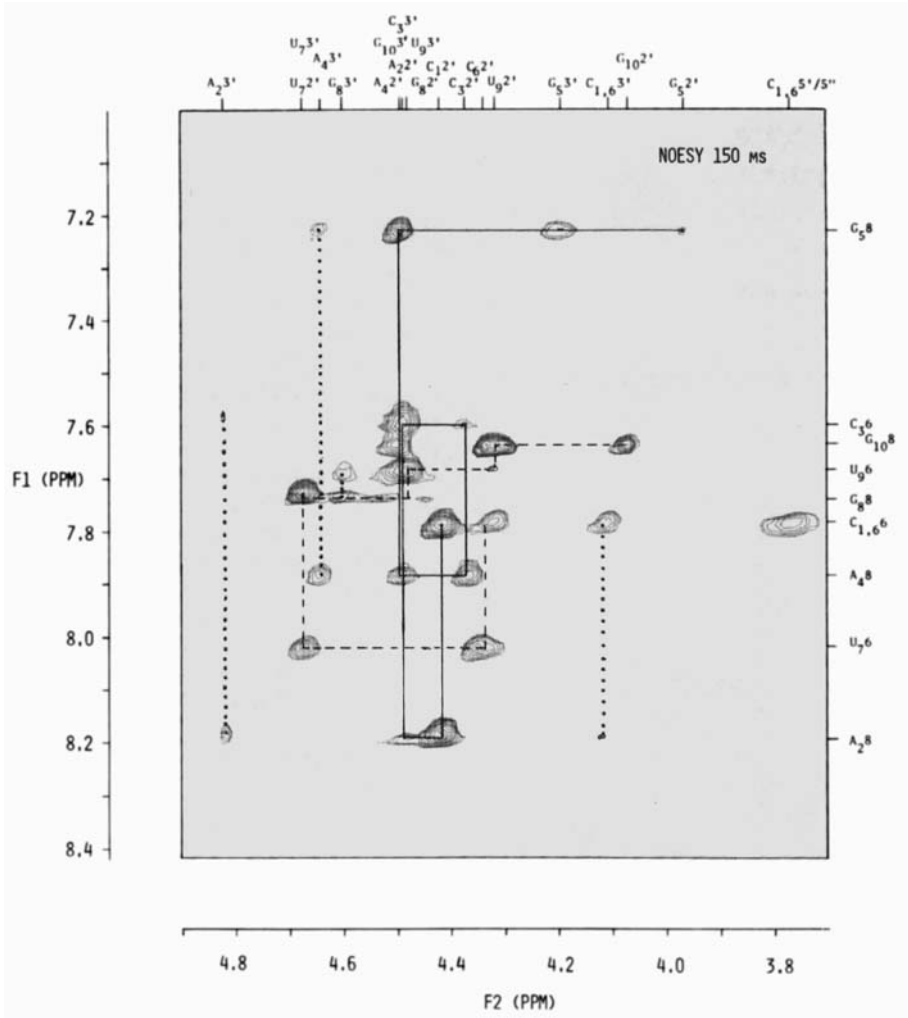

Fig. 4. *H8/H6 (F1 axis)-H2′/H3′/H4′/H5′/H5″ (F2 axis) region of the pure-phase absorption NOESY spectrum at a mixing time of 150 ms.* The H2′(*i*-1)-H8/H6(*i*)-H2′(*i*) connectivities are shown as continuous (——) and interrupted (– – –) lines for strands 1 and 2 respectively. Some H3′(*i*-1)-H8/H6(*i*) connectivities are represented by dotted lines (· · · · ·). Apodization was carried out by multiplying the time-domain data with a sine-squared bell shifted by $\pi/6$ in both t_1 and t_2 dimensions

the 3′-*endo* conformation characteristic of A-RNA, and a maximum value of about 0.29 nm when the sugar pucker is in the 2′-*endo* conformation. The values we obtain using the H5-H6 base vector as an internal reference lie within 0.25–0.27 nm (see Table 2). If the effective correlation time of the sugar moieties were significantly shorter than that of the bases, then these values of $r_{H1'(i)\text{-}H2'(i)}$ would represent overestimates. This, however, clearly cannot be the case on stereochemical grounds. That the internal mobility of the sugar and base moieties is the same in RNA, in contrast to the situation in DNA, is not surprising as the mobility of the ribose ring in RNA would be expected to be considerably reduced relative to that of the deoxyribose ring in DNA, first on account of steric hindrance arising from the presence of the bulky 2′-hydroxyl group on the ribose and second due to electrostatic interactions between this group of residue *i* and the O4′ atom of residue $i+1$, immobilizing one ribose ring with respect to the neighbouring ones.

A summary of the interproton cross-relaxation rates that could be measured together with the distances calculated from

Table 1. *Assignments of the non-exchangeable protons of the duplex RNA pentamers*
Chemical shifts at 21 °C are quoted from 4,4-dimethylsilapentane-1-sulfonate

Strand	Residue	Chemical shift of						
		H8/H6	H5	H2	H1′	H2′	H3′	H4′
		ppm						
1.	C_1	7.78	5.75		4.97	4.38	4.09	4.06
	A_2	8.19		7.43	5.92	4.46	4.80	4.37
	C_3	7.60	5.20		5.41	4.37	4.46	4.46
	A_4	7.89		7.06	5.86	4.47	4.62	4.63
	G_5	7.24			5.67	3.96	4.16	4.18
2.	C_6	7.78	5.79		4.99	4.33	4.09	4.08
	U_7	8.04	5.37		5.56	4.65	4.65	4.42
	G_8	7.74			5.78	4.45	4.57	4.60
	U_9	7.70	5.09		5.44	4.32	4.45	4.49
	G_{10}	7.65			5.83	4.08	4.47	4.29

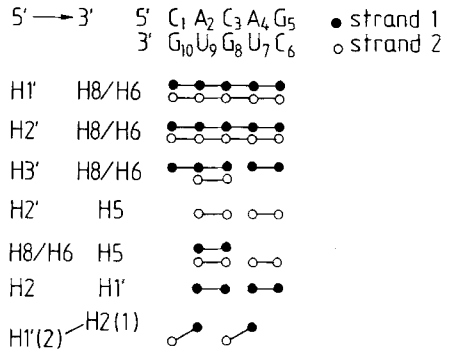

Fig. 5. *Summary of the internucleotide NOEs observed for the duplex RNA*

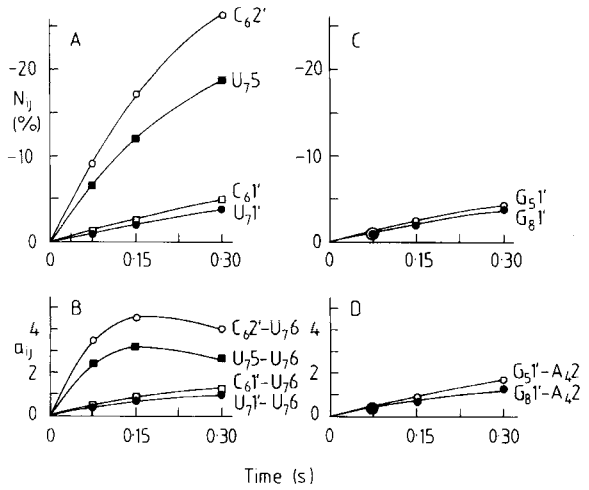

Fig. 6. *Time dependence of one-dimensional NOEs* N_{ij} *observed on irradiating the* $U_7(H6)$ *(A) and* $A_4(H2)$ *resonances (C).* The time dependence of the intensities of the corresponding cross-peaks a_{ij} (in arbitrary units) in the pure-phase absorption NOESY spectra are shown in (B) and (D) respectively. The intensities of the cross-peaks were obtained by two-dimensional integration from NOESY spectra for which the time-domain data had been multiplied by an exponential equivalent to a line-broadening of 2 Hz in both t_1 and t_2 dimensions. It can be seen that the ratios of the initial slopes of the time development of the NOEs measured from one-dimensional spectra and of the cross-peaks measured from the NOESY spectra are identical within experimental error

them is given in Table 2. Taking into account both cautionary considerations discussed above as well as experimental errors, we estimate that the error in the values of the calculated distances is in general $\lesssim$ 0.02 nm. However, in the case where the estimated distances are greater than about 0.33 nm, the errors may be somewhat larger with the values of the calculated interproton distance underestimated by $\lesssim$ 0.03 nm.

Refinement of the solution structure of the RNA pentamer

The refinement of macromolecular structures on the basis of interproton distances determined by NOE measurements is characterized by a poor observation-to-parameter ratio. A satisfactory refinement must therefore call upon other sources of information, in particular the stereochemical restraints on a molecule which arise from energy considerations. A similar problem is met in protein crystallography where the reduced degree of order in crystals relative to small molecule crystals leads to higher thermal or discorder diffuse scattering and to Bragg reflections which only extend to a limited resolution. As a result many protein crystals do not diffract to better than 0.25 nm (compared to less than 0.1 nm for small molecule crystals) so that the number of structure amplitudes from the crystal becomes equal to the number of positional parameters [26]. Given these similarities, the approach we have chosen for refinement of the RNA pentamer, and which has previously been applied successfully to the refinement of the solution structures of the B-DNA undecamer 5'd(AAGTGTGACAT) · 5'd(ATGTCACACTT) [13] and the B-DNA hexamer 5'd(CGTACG)$_2$ [47], is based on a crystallographic restrained least-squares refinement using the program RESTRAIN [25–27]. Examples of protein crystal structures refined using RESTRAIN include ribonuclease A [49], avian pancreatic polypeptide [50, 51] and γ-crystallin [52, 53]. Other approaches that have been used to achieve the same end goal, namely the determination of the three-dimensional solution structure of a macromolecule or of a ligand bound to a macromolecule on the basis of interproton distance data determined from NOE measurements, include model building and molecular graphics [14, 41], the use of distance geometry algorithms based on triangulation [54–56] and the use of restrained molecular dynamics calculations [57] (and GMC, AMG, A. T. Brünger, L. Nilsson & M. Karplus, in preparation).

The function minimized in cartesian coordinate space is given by

$$C = \Sigma W_d (d_t - d_c)^2 + \Sigma W_v |V| + \Sigma W_b (b_0 - b_{\min})^2 \quad (b_0 < b_{\min}) \qquad (2)$$

where W_d, W_v and W_b are weighting coefficients, d_t and d_c are the target and calculated interatomic distances respectively, $|V|$ is the determinant of the product-moment matrix for planar groups of atoms (the necessary and sufficient condition for a set of atoms to be planar being that $|V|$ is zero), and b_0 and $b_{\min}$ are calculated and minimum allowed distances between two non-bonded atoms. ($b_{\min}$ is the sum of the van der Waals radii for pairs of non-bonded atoms and the values of the van der Waals radii used are as follows: H, 0.1 nm; C, 0.16 nm; N, 0.145 nm; O, 0.135 nm; and P, 0.18 nm.) The last term in Eqn (2) is simply used to prevent undesirably close contacts and only comes into operation when $b_0 < b_{\min}$. The interatomic distances include all distances between covalently bonded atoms, between atoms defining fixed bond angles, and between atoms defining hydrogen bonding in A · U and G · C base pairs, as well as the experimental interproton distances determined from the NOE measurements. The geometric restraint terms correspond to the central force field approximation in vibrational spectroscopy with the force constants crudely approximated by assuming the same value for all non-bonded distances ($r < 0.212$ nm), another value for atoms separated by two bonds (0.212 nm $< r <$ 0.26 nm), and a third value for pairs separated by three bonds ($r > 0.26$ nm). The values of these geometric distance restraints are based on standard bond lengths and angles. The weights for these three geometric distance ranges are also applied to the interproton and hydrogen bonding distances. For planar groups of atoms the central force field is inadequate for maintaining the geometry imposed by a π-electron delocalization. Planar restraints in geometric least squares can be applied in one of three ways: by positioning a dummy atom at some distance from the plane [58], by minimizing the current least-squares best plane [59] or by minimizing the

Table 2. *Cross-relaxation rates for the RNA pentamer determined from time-dependent NOE measurements together with the* $(\langle r^{-6}\rangle)^{-1/6}$ *mean interproton distances calculated from them*

The relative errors in the values of the cross-relaxation rate are $\lesssim$ 15%. The $(\langle r^{-6}\rangle)^{-1/6}$ mean interproton distances are calculated using the distance (0.246 nm) and mean cross-relaxation rate between the H5 and H6 protons of the C and U residues. Assuming an error of $\pm$ 0.005 nm in the value of the reference distance (calculated on the basis of standard bond lengths and angles), the error in the values of the calculated distances is $\lesssim$ 0.02 nm for $r \lesssim$ 0.33 nm and $\lesssim$ 0.03 nm for 0.33 nm $\lesssim r \lesssim$ 0.4 nm

(A) *Intranucleotide*

Strand	Residue	H1′-H8/H6		H2′-H8/H6		H3′-H8/H6		H1′-H2′		H5-H6	
		σ_{ij}	r_{ij}	σ_{ij}	r_{ij}	σ_{ij}	r_{ij}	σ_{ij}	r_{ij}	σ_{ij}	r_{ij}
		s^{-1}	nm	s^{-1}	nm	s^{-1}	nm	s^{-1}	nm	s^{-1}	nm
1.	C_1	0.15	0.34					0.90	0.25	0.90	0.25
	A_2	0.26	0.31	0.36	0.29	0.71	0.26				
	C_3	0.17	0.33	0.89	0.25					0.85	0.25
	A_4	0.10	0.36			0.32	0.30				
	G_5	0.12	0.35	0.30	0.30	0.60	0.27	0.67	0.27		
2.	C_6	0.20	0.32					0.89	0.25	1.10	0.25
	U_7	0.12	0.35					0.85	0.25	0.92	0.25
	G_8	0.13	0.35			0.60	0.27	0.86	0.25		
	U_9	0.18	0.33	0.64	0.27			0.70	0.26	1.02	0.25
	G_{10}	0.19	0.33	0.86	0.25			0.88	0.25		

(B) *Internucleotide (interstrand)*

Strand	Residues	Proton residue i — proton residue $(i+1)$													
		H1′-H8/H6		H2′-H8/H6		H3′-H8/H6		H1′-H5		H2′-H5		H8/H6-H5		H2-H1′	
		σ_{ij}	r_{ij}	σ_{ij}	r_{ij}	σ_{ij}	r_{ij}	σ_{ij}	r_{ij}	σ_{ij}	r_{ij}	σ_{ij}	r_{ij}	σ_{ij}	r_{ij}
		s^{-1}	nm	s^{-1}	nm	s^{-1}	nm	s^{-1}	nm	s^{-1}	nm	s^{-1}	nm	s^{-1}	nm
1.	C_1pA_2	0.19	0.33	2.5	0.21	0.36	0.29								
	A_2pC_3	0.16	0.34			0.37	0.29	0.10	0.36	0.90	0.25	0.13	0.35	0.12	0.35
	C_3pA_4	0.13	0.35	1.0	0.25										
	A_4pG_5	0.12	0.35	1.0	0.25									0.12	0.35
2.	C_6pU_7	0.15	0.34	1.2	0.24					1.3	0.24	0.36	0.29		
	U_7pG_8	0.13	0.35	1.5	0.23										
	G_8pU_9	0.18	0.33			0.76	0.26	0.11	0.36	1.0	0.25	0.32	0.30		
	U_9pG_{10}	0.19	0.33	2.2	0.22										

(C) *Internucleotide (unterstrand)*

Residues	Strand 1 — strand 2 H2 — H1′	
	σ_{ij}	r_{ij}
	s^{-1}	nm
A_2-G_{10}	0.12	0.35
A_4-G_8	0.12	0.35

determinant of the product-moment matrix for planar groups of atoms, where the matrix V is given by

$$V = \begin{bmatrix} \Sigma x_i x_i & \Sigma x_i y_i & \Sigma x_i z_i \\ \Sigma y_i x_i & \Sigma y_i y_i & \Sigma y_i z_i \\ \Sigma z_i x_i & \Sigma z_i y_i & \Sigma z_i z_i \end{bmatrix}. \quad (3)$$

The first two methods not only restrain the atoms to be planar but also restrain them to the current least-squares plane. In contrast, the third method does not dampen changes in orientation of the plane produced by the other terms in Eqn (2) [25, 26]. The pseudo-force constant associated with the determinant $|V|$ may be chosen to yield RMS deviations from the refined least squares plane of $\lesssim$ 0.002 nm. In the present case the C1′ atom of the ribose and all the atoms of the base for each residue were constrained to lie in the same plane.

It should be borne in mind that the restrained least-squares refinement used here is quite distinct from a full-scale energy refinement. In particular it is important to note that the change in conformation on restrained least-squares refinement, in contrast to the case for energy refinement, arises solely from the interproton distance restraints, as all the other restraints are well satisfied in the initial and final structures as well as in the intermediate structures sampled during the entire course of the refinement.

Table 3. *RMS difference between the target restraints and the corresponding calculated values for initial RNA models I and II and the final refined structures I and II of the RNA pentamer*

Initial RNA model I is derived from the fibre diffraction data of Arnott et al. [60] subjected to five cycles of regularization (i.e. minimization using all restraints with the exception of non-bonded contact and experimental interproton distance restraints). Initial RNA model II was obtained by subjecting initial RNA model I to ten further cycles of regularization including non-bonded contact restraints. It should be noted that bond angles are defined by interatomic distances. For each residue the C1′ atom of the ribose and all the atoms of the base are constrained to lie in the same plane. The base-pairing restraints are as follows: for A · U base pairs, $r_{A(N6)\text{-}U(O4)} = 0.295$ nm, $r_{A(HN')\text{-}U(O4)} = 0.187$ nm, $r_{A(N1)\text{-}U(H3)} = 0.174$ nm, $r_{A(N1)\text{-}U(N3)} = 0.282$ nm, and $r_{A(H2)\text{-}U(H3)} = 0.287$ nm; for G · C base pairs, $r_{G(O6)\text{-}C(N4)} = 0.291$ nm, $r_{G(O6)\text{-}C(HN')} = 0.183$ nm, $r_{G(N1)\text{-}C(N3)} = 0.295$ nm, $r_{G(H1)\text{-}C(N3)} = 0.187$ nm, $r_{G(H1)\text{-}C(HN')} = 0.271$ nm, $r_{G(N2)\text{-}C(O2)} = 0.286$ nm and $r_{G(HN')\text{-}C(O2)} = 0.178$ nm. These values were obtained from the X-ray crystal structure analyses of ApU [61] and GpC [62]. The interproton distances given do not include the intranucleotide $r_{H5\text{-}H6}$ distances which are fixed by the geometry of the C and U bases themselves

Parameter	Number of restraints	RMS difference			
		initial RNA models		final refined structures	
		I	II	I	II
		nm			
All distances					
$r < 0.212$ nm	459	0.0067	0.0114	0.0035	0.0035
0.212 nm $< r <$ 0.26 nm	485	0.0113	0.0107	0.0054	0.0054
$r > 0.26$ nm	64	0.0537	0.0627	0.0182	0.0174
Covalent and bond angle restraints					
$r < 0.212$ nm	444	0.0014	0.0016	0.0035	0.0034
0.212 nm $< r <$ 0.26 nm	468	0.0021	0.0026	0.0051	0.0052
$r > 0.26$ nm	10	0.0016	0.0011	0.0013	0.0018
Planes	10	0.0005	0.0010	0.0015	0.0017
Base-pairing restraints	31	0.0250	0.0510	0.0096	0.0086
Interproton distances	55	0.0667	0.0716	0.0193	0.0186
Other values					
Total number of atoms	311 (927 degrees of freedom)				
Total number of restraints	1018				
Overall RMS shifts:					
initial I vs initial II:	0.025 nm				
initial I vs refined I:	0.040 nm				
initial II vs refined II:	0.052 nm				
refined I vs refined II:	0.011 nm				

Taking into account the fact that the geometric restraints (*viz.* bond lengths and angles) are conformation-independent, the conformation of the pentamer can be described by a total of 62 torsion angles comprising the glycosidic (χ) and main chain (α to ξ) torsion angles, subject to additional base pairing restraints. Thus, in torsion angle space there are a total of 86 distance restraints (55 experimental interproton distances and 31 further distances defining A · U and G · C base pairing; see Table 3) to determine 62 torsion angles. In cartesian coordinate space, where all the positional parameters need to be considered, we have a total of 1018 restraints for 927 degrees of freedom.

Two refinements were carried out. For the first refinement, the starting coordinates, known as initial RNA model I, were those of classical A-RNA derived from the fibre diffraction data of Arnott et al. [60] subjected to five cycles of regularization (i.e. minimization using all restraints with the exception of non-bonded contact and experimental interproton distance restraints). For the second refinement, the starting coordinates, known as initial RNA model II, were obtained by subjecting the coordinates for initial RNA model I to 10 further cycles of regularization including non-bonded contact restraints. For both refinements the weightings for the three distance ranges $r < 0.212$ nm, 0.212 nm $< r <$ 0.26 nm and $r > 0.26$ nm, and planes were applied throughout in the ratio of 5:4:3:4. These distance weights were chosen to represent approximately the gradation of error as a function of distance for the experimental interproton distances. For the first 10 cycles of refinement the non-bonded contact restraints were included; thereafter, they were switched off. In total, 35 cycles of refinement were performed.

The RMS difference between the target and calculated values for the distance and planarity restraints in the initial and final structures is given in Table 3 together with the overall RMS shifts between the structures. The average RMS differences in the coordinates of the sugar-phosphate and base moieties between the structures are plotted as a function of residue number in Fig. 7. It is clear from the data in Table 3 that the refinement has maintained good agreement for the geometric, planarity and base-pairing restraints, and resulted in a considerable improvement in the agreement between calculated and target interproton distances. Thus the RMS difference between calculated and measured interproton distances has fallen from 0.067 nm and 0.072 nm in initial

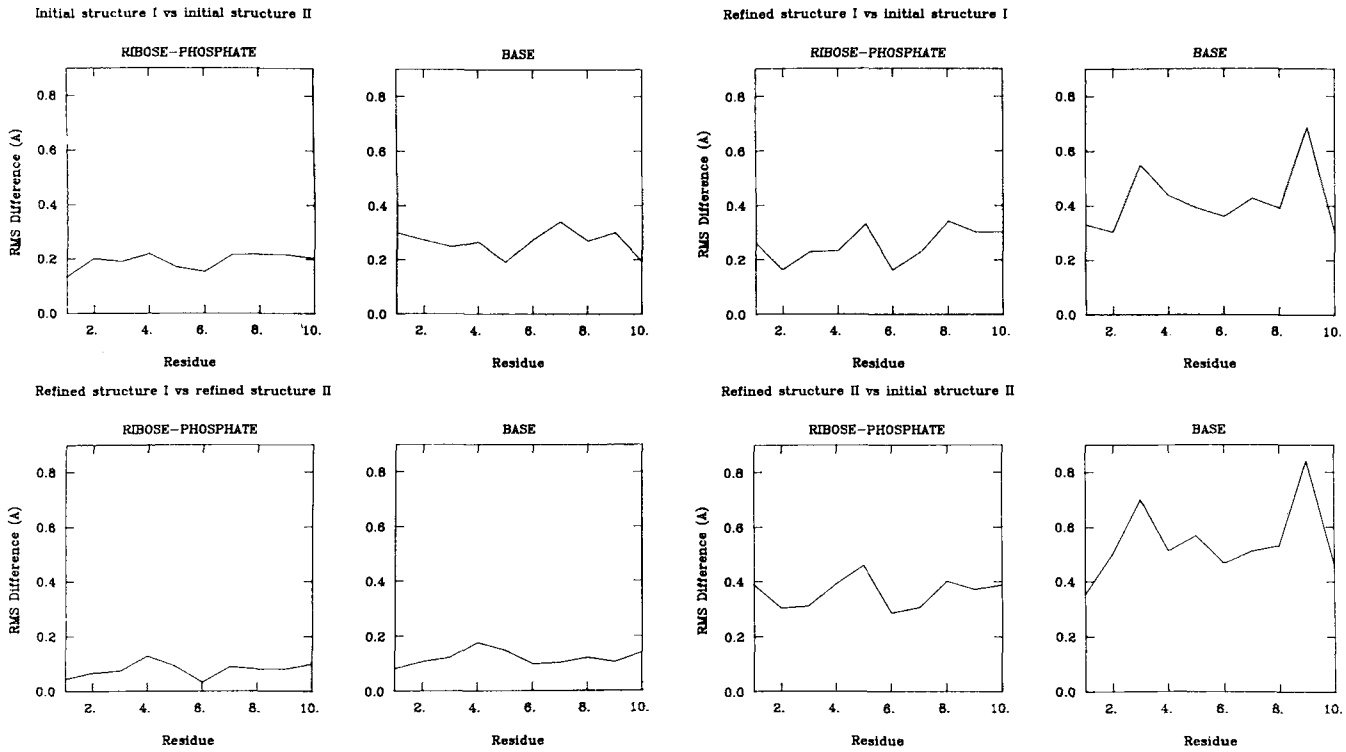

Fig. 7. *Variations in RMS difference for the sugar-phosphate and base moieties between the initial and refined structures of the RNA pentamer as a function of residue number.* Values of the RMS difference are given in Å (1 Å ≡ 0.1 nm)

structures I and II, respectively, to 0.019 nm in the final refined structures I and II, which is comparable to the error in the experimental data (on average $\lesssim$ 0.02 nm as discussed previously). In addition, there are no undesirably close contacts (i.e. van der Waals violations greater than 0.05 nm) in the refined structures. It can also be seen from Table 3 and Fig. 7 that the RMS difference between the two refined structures (0.011 nm) is small and approximately a factor of 2.5 less than that between the two initial structures. Indeed, when superimposed the two refined structures are virtually indistinguishable. The similarity between the two refined structures is further demonstrated by the agreement between the conformational parameters listed in Tables 4 and 5. A word of caution, however, should be added here. Although the striking similarity of the two refined structures provides a good measure of the convergence of the refinement method within say a range of $\lesssim$ 0.1 nm, the existence of a different structure outside this convergence range which could equally well account for the experimental interproton distance data can never be excluded. However, given that the RMS difference between calculated and experimental interproton distances for the two refined structures presented here is within experimental error, there would be no basis for preferentially choosing a putative third structure from the present two, even if this third structure exhibited an even better agreement between calculated and experimental distances. Nevertheless, we believe that considerable confidence can be placed in the refined structures presented here as they were derived from eminently reasonable starting models derived on the basis of a qualitative interpretation of the NOE data as well as a CD spectrum, namely standard A-RNA.

Because the solution structure is dynamic rather than static, the measured interproton distances, which are $(\langle r^{-6}\rangle)^{-1/6}$ means, are invariably weighted towards fluctuations with the shortest interproton distances. Hence, the average solution structure produced on refinement is neither a linear superposition of structures as in X-ray crystallography nor an arithmetic time average but an $(\langle r^{-6}\rangle)^{-1/6}$ time average in cartesian coordinate space. Such a structure could potentially be distorted relative to the arithmetic time-average structure. However, the refinement itself provides information both on the magnitudes of the internal motions and the relationship of the $(\langle r^{-6}\rangle)^{-1/6}$ time-averaged refined structures to the arithmetic time-averaged solution structure. This is because many of the interproton distances are correlated (*viz.* for three successives residues all intranucleotide and internucleotide distances are correlated so that a conformational change resulting in an alteration in one distance will inevitably result in alterations in other distances as well) and, hence, a single structure would not be able to provide an adequate fit to the experimental data if the magnitude of the internal motions is large [13, 48]. In the present case, the magnitude of the internal motions must be small in order to accomodate an RMS difference of only 0.019 nm between the experimental and calculated interproton distances for the two refined structures. Thus, we conclude that the $(\langle r^{-6}\rangle)^{-1/6}$ time average which the two refined structures represent is close to the arithmetic time-averaged structure and that the small RMS difference between the two refined structures (0.011 nm) provides a measure of the error in the refined coordinates.

Three stereo views of refined structure II are shown in Fig. 8 and the conformational parameters describing the refined structures are given in Tables 4 and 5. It is clear from this data that although the overall structural framework is that of A-RNA with the values of the glycosidic bond and

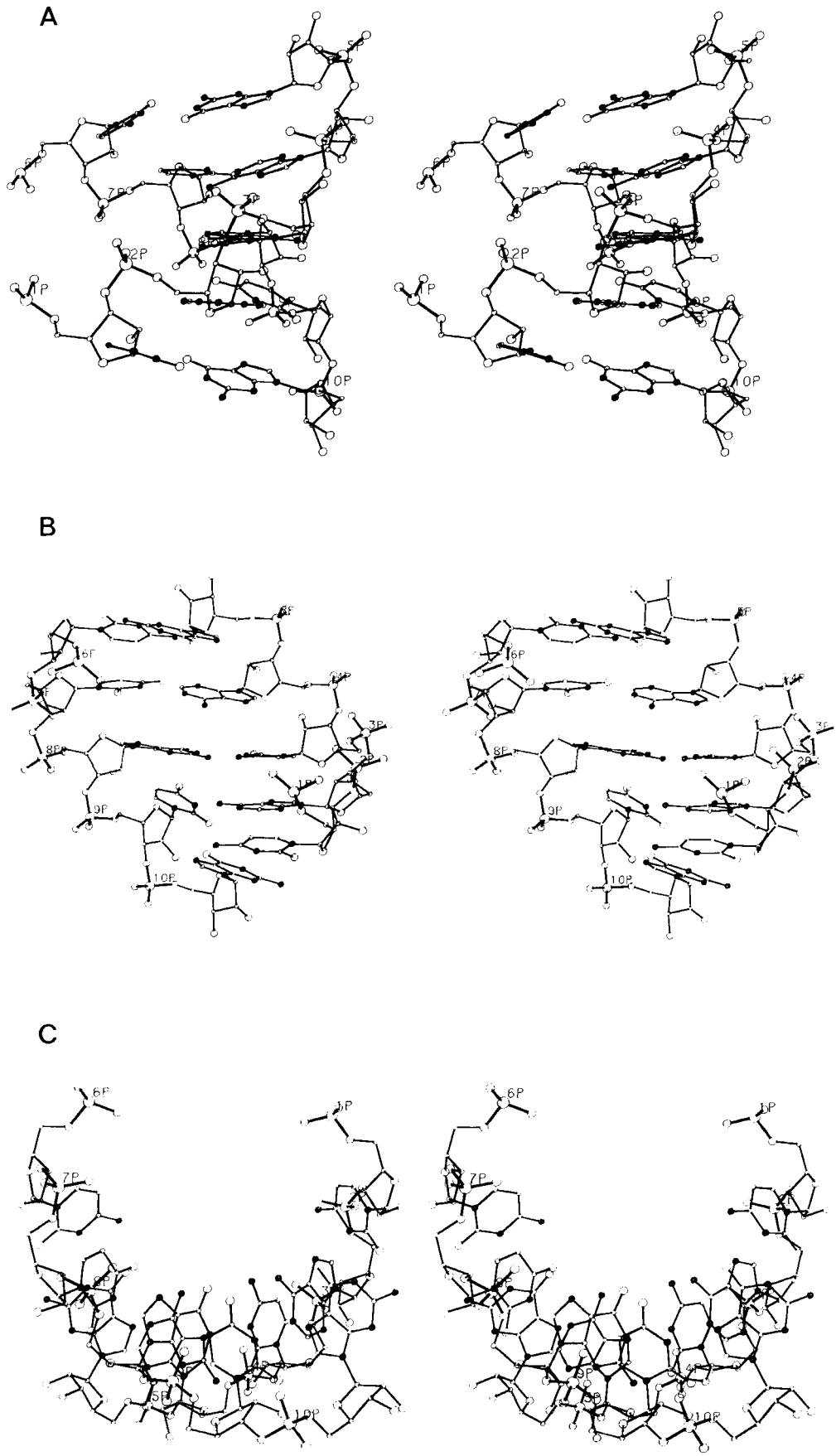

Fig. 8. *Three stereoviews of refined structure II of the RNA pentamer.* In (A) and (B) the structure is viewed along the helix and in (B) the view looks directly into the major groove. In (C) the structure is viewed down the helix axis. For the sake of clarity, protons have been omitted. Because refined structures I and II are virtually indistinguishable only one structure is shown

Table 4. *Torsion and propellor twist angles, separation between adjacent phosphorus atoms and distances between the O2′ atom of residue* i *and the O4′ atom of the adjacent 3′-residue for the refined structure I and II of the RNA pentamer*

The main chain torsion angles are defined by $P\overset{\alpha}{-}O5'\overset{\beta}{-}C5'\overset{\gamma}{-}C4'\overset{\delta}{-}C3'\overset{\varepsilon}{-}O3'\overset{\xi}{-}P$ and the glycosidic bond torsion angles by χ_{pur} = O1′-C1′-N9-C4 for purines and χ_{pyr} = O1′-C1′-N1-C2 for pyrimidines with zero at the *cis* position and positive angles by clockwise rotation of the further pair of atoms. The propellor twist angle ψ is the dihedral angle between individual base planes. Parameters for initial RNA models I and II are given (see Table 3). Values for A_c-DNA are from the crystal data of Shakked et al. [63] on the self-complementary A-DNA octamer $d(GGTATACC)_2$ and from the crystal data of Conner et al. [64] on the self-complementary A-DNA tetramer $d(CCGG)_2$. Values for tRNA are for the TΨC stem (residues 49–53 and 65–69) of yeast $tRNA^{Phe}$ derived from the monoclinic ($tRNA_M$) [65] and orthorhombic ($tRNA_O$) [66] crystal structures. In the case of $tRNA_M$, the mean values of α and ξ do not include those for residue 49; in the case of $tRNA_O$, the mean value of α does not include those for residues 49, 50 and 61, the mean value of γ those for residues 50, 61 and 65, and the mean value of ξ that for residue 49, as in all these cases large departures (> 50°) from the values for the other residues are found

Strand	Residue	Refined structure I/refined structure II										Sugar pucker
		glycosyl χ	backbone torsion angles						phosphorus atom separation	$r_{O2'(i)\text{-}O4'(i+1)}$	propellor twist Ψ	
			α	β	γ	δ	ε	ξ				
		degrees							nm		deg.	
1.	C_1	−144/−144	−	−	47/46	75/75	176/178	−42/−42	0.56/0.56	0.41/0.40	15/15	C3′-*endo*
	A_2	−156/−158	−88/−83	−157/−164	47/45	77/75	173/172	−50/−50	0.56/0.55	0.31/0.31	21/20	C3′-*endo*
	C_3	−158/−159	−83/−84	−161/−165	46/47	97/97	184/189	−70/−75	0.56/0.56	0.30/0.30	11/9	O1′-*endo*
	A_4	−152/−153	−78/−79	−163/−169	49/53	80/74	181/185	−50/−51	0.57/0.58	0.41/0.41	24/22	C3′-*endo*
	G_5	−166/−170	−83/−76	−165/−175	48/43	82/82	−	−	−	−	2/0	C3′-*endo*
2.	C_6	−139/−137	−	−	53/53	90/89	178/177	−60/−60	0.58/0.58	0.34/0.36	2/0	O1′-*endo*
	U_7	−148/−151	−85/−91	−150/−150	47/51	81/79	171/173	−40/−41	0.56/0.57	0.42/0.43	24/22	C3′-*endo*
	G_8	−157/−160	−95/−89	−152/−157	54/52	74/75	188/190	−59/−63	0.56/0.56	0.34/0.34	11/9	C3′-*endo*
	U_9	−162/−162	−74/−72	−167/−169	42/43	108/108	176/175	−79/−73	0.56/0.56	0.30/0.30	21/20	O1′-*endo*
	G_{10}	−167/−171	−81/−86	−162/−162	52/59	78/75	−	−	−	−	15/15	C3′-*endo*
	mean	−156 ± 10	−83 ± 6	−162 ± 7	49 ± 4	84 ± 11	179 ± 6	−57 ± 13	0.57 ± 0.01	0.35 ± 0.05	14 ± 8	C3′-*endo*
A-RNA I		−154	−85	−152	47	81	180	−47	0.565	0.340	−	C3′-*endo*
A-RNA II		−155 ± 2	−80 ± 3	−165 ± 6	47 ± 3	82 ± 3	−179 ± 1	−56 ± 1	0.568 ± 0.004	0.389 ± 0.01	−	C3′-*endo*
A_c-DNA [63]		−160 ± 8	−62 ± 12	173 ± 8	52 ± 14	88 ± 3	−152 ± 8	−78 ± 7			13 ± 4	C3′-*endo*
A_c-DNA [64]		−157 ± 14	−73 ± 4	−179 ± 9	73 ± 30	89 ± 25	−161 ± 7	−66 ± 5			16 ± 4	C3′-*endo*
$tRNA_M$ [65]		−169 ± 7	−79 ± 7	−180 ± 13	67 ± 11	82 ± 3	−159 ± 6	−70 ± 6			4	C3′-*endo*
$tRNA_O$ [66]		−182 ± 26	−79 ± 21	160 ± 20	64 ± 19	82 ± 4	−138 ± 21	−80 ± 17			10 ± 7	C3′-*endo*

Table 5. *Rise per base pair (h) and local helical twist (t_1), base roll (θ_R) and base tilt (θ_T) angles for refined structures I and II of the RNA pentamer*

The base roll angle θ_R is the rotation about an axis in the plane of the bases perpendicular to the pseudo-dyad and is positive when opening towards the minor groove. The base tilt angle θ_T is the rotation about the pseudo-dyad axis passing through the base plane and is positive when opening to the outside of the molecule. θ is the magnitude of the total angle between successive base plane normals and is given by $\sin^{-1}[(\sin^2\theta_R + \sin^2\theta_t)^{1/2}]$. Parameters are also given for initial RNA model I (see Table 3). Values for A_c-DNA are from the crystal data of Shakked et al. [63] or the crystal data of Conner et al. [64]. Values for tRNA are for the TΨC stem (residues 49–53 and 65–69) of yeast $tRNA^{Phe}$ derived from the monoclinic ($tRNA_M$) [65] and orthorhombic ($tRNA_O$) [66] crystal structures

Base pair step	Refined structure I/refined structure II							
	h	t_1	strand 1			strand 2		
			θ	θ_R	θ_T	θ	θ_R	θ_T
	nm	degrees						
1 C_1G_{10}-A_2U_9	0.22/0.24	30/30	12/12	12/12	−1/−2	4/4	−3/−2	2/4
2 A_2U_9-C_3G_8	0.27/0.27	31/31	12/11	12/11	1/0	18/15	16/13	−7/−8
3 C_3G_8-A_4U_7	0.24/0.23	30/30	12/16	12/15	0/4	17/18	1/1	17/18
4 A_4U_7-G_5C_6	0.24/0.25	31/31	5/5	0/1	−5/−5	33/36	32/35	−6/−6
mean	0.25 ± 0.02	30.5 ± 0.5	11 ± 4	9 ± 6	−1 ± 3	18 ± 12	12 ± 15	2 ± 11
A-RNA I	0.26	30						
A_c-DNA [63]	0.30 ± 0.04	32.2 ± 2						
A_c-DNA [64]	0.29	33.7						
$tRNA_M$ [65]	0.255	32.9						
$tRNA_O$ [66]	0.258 ± 0.01	33.1 ± 1.4						

backbone torsion angles lying within the range characteristic of A-RNA, the refined structures are far from regular. For example, propeller twist angles range from 0° to 24°, base roll angles from −3° to +35°, glycosidic bond torsion angles from −137° to −171°, C4′-C3′ bond torsion angles from 75° to 108°, O3′-P bond torsion angles from −40° to −79°, and so on. This spread is similar to that observed in the crystal structures of the A-DNA octamer 5′d(GGTATACC)$_2$ [63] and tetramer 5′d(CCGG)$_2$ [64], as well as in the TΨC stem of the monoclinic [65] and orthorhombic [66] crystal structures of $tRNA^{Phe}$. Another feature of interest concerns the distance between the O2′ atom of the 5′-residue and the O4′-atom of the 3′-residue which has a spread of values over 0.29–0.41 nm. In three cases, namely base steps A_2pC_3, C_3pA_4 and U_9pG_{10}, this distance has a value of about 0.3 nm which would be consistent with the formation of O2′H · O4′ hydrogen bonds. For the other base steps the $r_{O2'(i)\text{-}O4'(i+1)}$ distance is sufficiently short to permit relatively strong electrostatic interactions.

Concluding remarks

In the present paper, we have presented the refinement of the solution structure of a RNA pentamer comprising one of the helical stems of yeast $tRNA^{Phe}$, namely the stem of the TΨC loop. Although the refined structure is clearly of the A-type, local structural variations are observed which cannot as yet be fitted to any generalized set of rules governing their sequence dependence. This was also found to be the case for the refined solution structures of a B-DNA undecamer [13] and a B-DNA hexamer [48]. In contrast, with the exception of a DNA · RNA hybrid [67], the local structural variations observed for the small number of A and B-DNA fragments crystallised to date seem to be reasonably well predicted by a set of simple sum functions [68] based on the avoidance of steric clash between purines on opposite strands of the helix at adjacent base pairs [69]. It therefore seems not unreasonable to conclude that the avoidance of this particular steric clash is not as important a factor in governing local structure in the solution state as in the crystal state. For example, with the exception of the fifth base pair $G_5 \cdot C_6$, all the base pairs are highly propellor twisted in the refined solution structure of the RNA pentamer (see Table 4). In structural terms, an increase in propellor twist leads to an increase in steric clash which is particularly marked in alternating pyrimidine(3′-5′)purine sequences such as the first four base pairs of the RNA pentamer. Indeed Dickerson's sum functions [68] predict that the first four base pairs should hardly be propellor twisted whereas the fifth base pair should show maximal propellor twist, exactly the opposite of what is observed. However, the observed propellor twisting may not in fact be all too surprising when one considers that an increase in propellor twist also leads to improved stacking interactions [70]. Thus, in this particular case in solution the energetic advantage of increased stacking may outweigh the disadvantage of some steric clash.

Whether or not a set of simple rules governing the sequence dependence of local structure, equivalent to those found in the crystal state, exists in solution is at present unknown as too few refined solution structures are available to date, although no doubt more will become available in the near future.

This work was supported by the *Max-Planck-Gesellschaft*. We are grateful to Thea Hellmann for technical assistance. The pentamer CUGUG was prepared by L. W. M. during the tenure of a short term EMBO fellowship in the laboratory of J. H. van Boom at the University of Leiden. The coordinates for the refined structures of the RNA pentamer are available on request.

REFERENCES

1. Patel, D. J., Pardi, A. & Itakura, K. (1982) *Science (Wash. DC) 216*, 581–590.
2. Patel, D. J., Kozlowski, S. A., Ikuta, S., Itakura, K., Bhalt, R. & Hare, B. R. (1983) *Cold Spring Harbor Symp. Quant. Biol. 47*, 197–206.
3. Kearns, D. R. (1984) *CRC Crit. Rev. Biochem. 15*, 237–290.

4. Clore, G. M. & Gronenborn, A. M. (1985) *FEBS Lett. 179*, 187–192.
5. Petersheim, M. & Turner, D. H. (1983) *Biochemistry 22*, 256–263.
6. Freier, S. M., Burger, B. J., Alkema, D., Neilson, T. & Turner, D. H. (1983) *Biochemistry 22*, 6198–6206.
7. Sinclair, A., Alkema, D., Bell, R. A., Coddington, J. M., Hughes, D. W., Neilson, T. & Romanink, P. J. (1984) *Biochemistry 23*, 2656–2662.
8. Clore, G. M., Gronenborn, A. M., Piper, E. A., McLaughlin, L. W., Graeser, E. & van Boom, J. H. (1984) *Biochem. J. 221*, 737–751.
9. Haasnoot, C. A. G., Westerink, H. P., van der Marel, G. A. & van Boom, J. H. (1984) *J. Biomol. Struct. Dynamics 2*, 345–360.
10. Reese, C. B. (1978) *Tetrahedon 34*, 3143–3175.
11. Van Boom, J. H. & Wreesman, C. T. J. (1984) in *Oligonucleotide synthesis: a practival approach* (Gait, M. J., ed.) pp. 153–183, IRL Press, Oxford.
12. Clore, G. M. & Gronenborn, A. M. (1984) *Eur. J. Biochem. 141*, 119–129.
13. Clore, G. M. & Gronenborn, A. M. (1985) *EMBO J. 4*, 829–835.
14. Clore, G. M., Gronenborn, A. M. & McLaughlin, L. W. (1984) *J. Mol. Biol. 174*, 163–173.
15. Gronenborn, A. M., Clore, G. M., McLaughlin, L. W., Graeser, E., Lorber, B. & Giegé, R. (1984) *Eur. J. Biochem. 145*, 359–364.
16. Gronenborn, A. M., Clore, G. M. & Kimber, B. J. (1984) *Biochem. J. 221*, 723–736.
17. Wreesman, C. T. J., Fidder, A., van der Marel, G. A. & van Boom, J. H. (1983) *Nucleic Acids Res. 11*, 8389–8405.
18. van der Marel, G. A., van Boeckel, C. A. A., Wille, B. & van Boom, J. H. (1982) *Nucleic Acids Res. 10*, 2337–2351.
19. McLaughlin, L. W. & Piel, N. (1984) in *Oligonucleotide synthesis: a practival approach* (Gait, M. J., ed.) pp. 117–133, IRL Press, Oxford.
20. McLaughlin, L. W. & Romaniuk, E. (1982) *Anal. Biochem. 124*, 37–44.
21. Jeener, J., Meier, B. H., Bachmann, P. & Ernst, R. R. (1979) *J. Chem. Phys. 71*, 4546–4553.
22. Marion, D. & Wüthrich, K. (1983) *Biochem. Biophys. Res. Commun. 113*, 967–974.
23. Macura, S., Huang, Y., Suter, D. & Ernst, R. R. (1981) *J. Magn. Reson. 43*, 259–281.
24. Dobson, C. M., Olejniczak, E. T., Poulsen, F. M. & Ratcliffe, R. G. (1982) *J. Magn. Reson. 48*, 97–110.
25. Moss, D. S. & Morffew, A. J. (1982) *Comput. Chem. 6*, 1–3.
26. Haaneef, I., Moss, D. S., Stanford, M. J. & Borkakoti, N. (1985) *Acta Crystallogr. A.*, in the press.
27. Haaneef, I., Moss, D. S., Stanford, M. J. & Borkakoti, N. (1983) *RESTRAIN user guide*, Birkbeck College, London.
28. Saenger, W. (1983) *Principles of nucleic acid structures*, Verlag Chemie, Weinheim.
29. Reid, D. G., Salisbury, S. A., Bellard, S., Shakked, Z. & Williams, D. H. (1983) *Biochemistry 22*, 2019–2025.
30. Reid, D. G., Salisbury, S. A., Brown, T., Williams, D. H., Vasseur, J. J., Rayner, B. & Imbach, J. L. (1983) *Eur. J. Biochem. 135*, 307–314.
31. Hare, D. R., Wemmer, D. E., Chou, S. H., Drobny, G. & Reid, B. R. (1983) *J. Mol. Biol. 171*, 319–336.
32. Scheek, R. M., Russo, N., Boelens, R., Kaptein, R. & van Boom, J. H. (1983) *J. Am. Chem. Soc. 105*, 2914–2916.
33. Scheek, R. M., Boelens, R., Russo, N., van Boom, J. H. & Kaptein, R. (1984) *Biochemistry 23*, 1371–1376.
34. Weiss, M. A., Patel, D. J., Sauer, R. T. & Karplus, M. (1984) *Proc. Natl Acad. Sci. USA 81*, 130–134.
35. Clore, G. M., Lauble, H., Frenkiel, T. A. & Gronenborn, A. M. (1984) *Eur. J. Biochem. 145*, 629–636.
36. Gronenborn, A. M. & Clore, G. M. (1985) *Prog. Nucl. Magn. Reson. Spectrosc. 17*, 1–32.
37. Wagner, G. & Wüthrich, K. (1979) *J. Magn. Reson. 33*, 675–680.
38. Macura, S. & Ernst, R. R. (1980) *Mol. Phys. 41*, 95–117.
39. Clore, G. M. & Gronenborn, A. M. (1985) *J. Magn. Reson. 61*, 158–164.
40. Poulsen, F. M., Hosch, J. C. & Dobson, C. J. (1980) *Biochemistry 19*, 2596–2607.
41. Senn, H., Billeter, M. & Wüthrich, K. (1984) *Eur. Biophys. J. 11*, 3–15.
42. Clore, G. M. & Gronenborn, A. M. (1985) in *Proceedings of the Fourth Conversation in Biomolecular Stereodynamics* (Sarma, R. H., ed.), Adenine Press, New York, in the press.
43. Clore, G. M. & Gronenborn, A. M. (1984) *FEBS Lett. 175*, 117–123.
44. Gronenborn, A. M. & Clore, G. M. (1982) *J. Mol. Biol. 157*, 155–160.
45. Clore, G. M. & Gronenborn, A. M. (1983) *J. Magn. Reson. 53*, 423–442.
46. Gronenborn, A. M., Clore, G. M., Brunori, M., Giardina, B., Falcioni, G. & Perutz, M. F. (1984) *J. Mol. Biol. 178*, 731–742.
47. Clore, G. M. & Gronenborn, A. M. (1984) *FEBS Lett. 172*, 219–225.
48. Clore, G. M., Gronenborn, A. M., Moss, D. S. & Tickle, I. J. (1985) *J. Mol. Biol. 184*, in the press.
49. Borkakoti, T., Palmer, R. A., Haneef, I. & Moss, D. S. (1983) *J. Mol. Biol. 169*, 743–755.
50. Blundell, T. L., Pitts, J. E., Tickle, I. J., Wood, S. P. & Wu, C. W. (1981) *Proc. Natl Acad. Sci. USA 78*, 4175–4179.
51. Glover, I., Haneef, I., Pitts, J., Wood, S. P., Moss, D. S., Tickle, I. J. & Blundell, T. L. (1983) *Biopolymers 22*, 293–304.
52. Blundell, T. L., Lindley, P. F., Miller, L., Moss, D. S., Slingsby, C., Tickle, I. J., Turnell, B. & Wistow, G. W. (1981) *Nature (Lond.) 289*, 771–777.
53. Blundell, T. L., Lindley, P. F., Miller, L., Moss, D. S., Slingsby, C., Tickle, I. J. & Wistow, G. W. (1981) *Acta Crystallogr. AS37*, 021–53.
54. Braun, W., Bösch, C., Brown, C. R., Go, N. & Wüthrich, K. (1981) *Biochim. Biophys. Acta 667*, 377–396.
55. Braun, W., Wider, G., Lee, K. H. & Wüthrich, K. (1983) *J. Mol. Biol. 169*, 921–948.
56. Arseniev, S. A., Kondakov, V. I., Maiorov, V. N. & Bystrov, V. J. (1984) *FEBS Lett. 165*, 57–62.
57. Kaptein, R., Zuiderweg, E. R. P., Scheek, R. M., Boelens, R. & van Gunsteren, W. S. (1985) *J. Mol. Biol. 182*, 179–182.
58. Dodson, E. J., Isaacs, N. W. & Rollet, J. S. (1976) *Acta Crystallogr. A32*, 311–315.
59. Hendrickson, W. A. & Konnert, J. H. (1980) in *Computing in crystallography*, Ch. 13, pp. 13.01–13.23, Indian Academy of Sciences, Bangalore.
60. Arnott, S., Hukins, D. W. L. & Dover, S. D. (1972) *Biochem. Biophys. Res. Commun. 48*, 1342–1399.
61. Seeman, N. C., Rosenberg, J. M., Suddath, F. L., Kim, J. J. P. & Rich, A. (1976) *J. Mol. Biol. 104*, 109–144.
62. Rosenberg, J. M., Seeman, N. C., Day, R. O. & Rich, A. (1976) *J. Mol. Biol. 104*, 145–167.
63. Shakked, Z., Rabinovich, D., Kennard, O., Cruse, W. B. T., Salisbury, S. A. & Viswamitra, M. A. (1983) *J. Mol. Biol. 166*, 183–201.
64. Conner, B. N., Yoon, C., Dickerson, J. L. & Dickerson, R. E. (1984) *J. Mol. Biol. 174*, 663–695.
65. Hingerty, B., Brown, R. S. & Jack, A. (1978) *J. Mol. Biol. 124*, 523–534.
66. Holbrook, S. R., Sussman, J. L., Warrant, R. W. & Kim, S. H. (1978) *J. Mol. Biol. 123*, 631–660.
67. Wang, A. H. J., Fujii, S., van Boom, J. H., van der Marel, G. A., van Boeckel, S. A. A. & Rich, A. (1982) *Nature (Lond.) 299*, 601–604.
68. Dickerson, R. E. (1984) *J. Mol. Biol. 166*, 419–441.
69. Calladine, C. R. (1982) *J. Mol. Biol. 161*, 343–352.
70. Levitt, M. (1978) *Proc. Natl Acad. Sci. USA 75*, 640–644.